Published in final edited form as:
Health Phys. 2015 April ; 108(4): 419–428. doi:10.1097/HP.0000000000000243.

Development and validation of a GEANT4 radiation transport code for CT dosimetry

DE Carver[*], **SD Kost**[†], **MJ Fernald**[‡], **KG Lewis II**[§], **ND Fraser**[**], **DR Pickens**[††], **RR Price**[‡‡], and **MG Stabin**[§§]

[*]Department of Radiology and Radiological Sciences, Vanderbilt University, 1161 21st Ave, Nashville, TN 37232

[†]Department of Radiology and Radiological Sciences, Vanderbilt University, 1161 21st Ave, Nashville, TN 37232

[‡]Rocky Mountain Oncology Center, 6501 E 2nd St, Casper, WY 82609

[§]Department of Radiology, Ochsner Medical Center, 1514 Jefferson Hwy, New Orleans, LA 70121

[**]Department of Radiology and Radiological Sciences, Vanderbilt University, 1161 21st Ave, Nashville, TN 37232

[††]Department of Radiology and Radiological Sciences, Vanderbilt University, 1161 21st Ave, Nashville, TN 37232

[‡‡]Department of Radiology and Radiological Sciences, Vanderbilt University, 1161 21st Ave, Nashville, TN 37232

[§§]Department of Radiology and Radiological Sciences, Vanderbilt University, 1161 21st Ave, Nashville, TN 37232

Abstract

We have created a radiation transport code using the GEANT4 Monte Carlo toolkit to simulate pediatric patients undergoing CT examinations. The focus of this paper is to validate our simulation with real-world physical dosimetry measurements using two independent techniques. Exposure measurements were made with a standard 100-mm CT pencil ionization chamber, and absorbed doses were also measured using optically stimulated luminescent (OSL) dosimeters. Measurements were made in air, a standard 16-cm acrylic head phantom, and a standard 32-cm acrylic body phantom. Physical dose measurements determined from the ionization chamber in air for 100 and 120 kVp beam energies were used to derive photon-fluence calibration factors. Both ion chamber and OSL measurement results provide useful comparisons in the validation of our Monte Carlo simulations. We found that simulated and measured CTDI values were within an overall average of 6% of each other.

For correspondence contact: Diana E. Carver, Department of Radiology and Radiological Sciences, Vanderbilt University, 1161 21st Ave, Nashville, TN 37232, call (615) 999-9626, or at diana.e.carver@vanderbilt.edu.

Keywords

Monte Carlo; computed tomography; dosimetry, external; diagnostic radiology

Introduction

Radiation dose calculations are essential to the understanding of the relationship between the risks and benefits of any medical examination. For younger subjects, concerns are heightened because of the greater radio-sensitivity of these individuals (Goske *et al.* 2008). The 2009 NCRP report on human population exposure to radiation noted a dramatic increase in the contributions of medical sources to our overall annual radiation exposure (Schauer and Linton 2009). Computed Tomography (CT) imaging now amounts to about 70% of the radiation dose delivered to patients undergoing medical examinations. It is estimated that CT procedures could account for as much as 60% of man-made radiation exposures to Americans (Linton and Mettler 2003).

Currently, the CT vendor-supplied CT dose index (CTDI) and dose-length-product (DLP) values for pediatric subjects are based on dose estimates derived from a standard 16-cm acrylic cylinder (AAPM Report 96 2008) and are assigned uniformly to all subjects (Dixon *et al.* 2003). A large amount of attention has been directed at radiation doses to pediatric patients since they comprise a particularly sensitive population (e.g. Brenner *et al.* 2001, Donnelly *et al.* 2001, Donnelly 2005, Dixon *et al.* 2003, Linton and Mettler 2003). The Alliance for Radiation Safety in Pediatric Imaging (http://www.pedrad.org/associations/5364/ig/) notes the need for special care in prescribing pediatric CT studies, encouraging scanning only areas necessary for evaluation, and reducing technique parameters (kVp and mAs) as much as possible (Donnelly *et al.* 2005, Goske *et al.* 2008). Medical professionals have noted the need for more accurate patient-specific dose values than are currently provided by the standardized manufacturer CT software (Strauss *et al.* 2009). There is also a great amount of effort to account for CT dose differences due to a patient's size (ICRP 102 2007, AAPM Report 96 2008, Goske *et al.* 2008).

In order to accurately estimate the risks from CT scans, one must be able to know the absorbed dose to each individual radiosensitive organ to determine effective dose (ICRP 60 1991, ICRP 103 2007). While there are methods to estimate effective dose from DLP (AAPM Report 96 2008), estimating individual organ doses relies on Monte Carlo simulations. There have been many endeavors to calculate organ and effective dose from CT exams using computational methods, (e.g. DeMarco *et al.* 2003, DeMarco *et al.* 2005, Jarry *et al.* 2003, Lee *et al.* 2007, Lee *et al.* 2008, Li *et al.* 2011a, Li *et al.* 2011b, Li *et al.* 2011c). These groups have validated their Monte Carlo methods against ionization chamber measurements in both cylindrical as well as anthropomorphic phantoms. Our work here applies similar validation methods using ionization chamber measurements to compare against OSL dosimeters (Landauer 2006).

Using the GEANT4 Monte Carlo toolkit (Agostinelli *et al.* 2003, Allison *et al.* 2006), we have created a radiation transport code to simulate patients undergoing exams on a CT scanner similar to that at Monroe Carrell, Jr. Children's Hospital at Vanderbilt. We used

measured values of dose from both ionization chamber measurements as well as optically stimulated luminescent (OSL) technology in physical phantoms to calibrate and validate the simulated output from our GEANT4 CT source. This paper provides a description of our Monte Carlo radiation transport code and our validation techniques

Methods

Monte Carlo Simulation of CT

GEANT4 (Agostinelli *et al.* 2003, Allison *et al.* 2006) is an open source, integrated software package that allows simulation of radiation transport for many particle types and many irradiation geometries. The toolkit provides a complete set of tools for all areas of detector simulation including geometry, tracking, physics models, and run and event management. The code includes all relevant physical processes governing particle interactions, stores and tracks event data, and permits the scoring of deposited energy and dose in selected target regions. The user must specify the specific characteristics of their simulation such as the detector geometry, materials, particles, physics processes, and primary events generation.

The detector geometry in our simulation consists of a nested parameterized 3D volume. One significant advantage of nested parameterization is the ability to assign each voxel unique material properties and chemical compositions. Energy deposition due to each primary event, including any secondary particles generated, is tallied for each voxel in the parameterized volume. Once all events are tracked, the simulation produces a map of the total energy deposited that is used to create a 3D dose map used to quantify the dose distribution within a particular region.

The parameterized 3D volume containing the voxels is positioned flush to an exam table. The physical exam table at Monroe Carrell, Jr. Children's Hospital at Vanderbilt was measured for size and thickness and modeled in our simulation geometry as a trapezoid with a thickness of 3 mm and height of 9 cm. The long and short sides measure 42 and 22 cm, respectively.

GEANT4 requires the user to define the particle type, position and direction vectors, and initial energy for each primary event. Primary photons must be generated to accurately represent the X-ray energy spectrum, bow-tie filtration, and source-to-isocenter geometry of the CT scanner. Source energy spectra were obtained for nominal beam energies typically used in pediatric protocols (100 and 120 kVp) and implemented in our simulation as look-up tables. A detailed description of the CT source model follows.

CT Source Model

To accurately model the CT scanner under consideration, comprehensive descriptions of the scanner properties including its photon energy spectrum, inherent and bow-tie filtration, and geometry are necessary. However, scanner-specific descriptions are normally proprietary and difficult to obtain through non-disclosure agreements. To overcome this limitation, we have taken numerous physical measurements and employed the methods of Turner *et al.* (2009) to generate an equivalent energy-fluence source model for the specific CT scanner in our simulation. Our fluence model also includes the effects of the body bow-tie filter that

provides X-ray filtration across the transverse direction of the patient to account for variations in body thickness.

All X-rays originate at the focal spot with energies determined by sampling the equivalent spectra across the bow-tie filter. These photons are given initial direction vectors to populate each angle in the fan beam with relative weights determined by the measured bow-tie filter attenuation profile (Fig. 2). It was assumed that the particle fluence was uniform in the scan direction, and photons are assigned uniformly random axial direction components. The full-width-half-max (FWHM) beam width measured at isocenter was used to define the beam collimation. The CT head moves in one-degree increments with 100,000 primary photons generated at each angle. The x-ray source rotates and translates helically based on a user-defined pitch until the entire range of the scan is complete. A detailed description of the measurements required to generate equivalent spectra for this specific CT scanner is provided in the following section.

Equivalent CT Source Modeling

We have modeled a third generation multi-detector array CT scanner (Philips Brilliance 64, Philips Healthcare, Andover, MA) with 64 rows of detectors of 0.625 mm each. X-ray beam collimations available for this particular scanner include 2 × 0.625 mm, 12 × 0.625 mm, 16 × 0.625 mm, and 64 × 0.625 mm. These beam collimations are reported as nT, where n is the number of detector elements, and T is the width of each detector element. The Philips Brilliance 64 has a source-to-isocenter distance of 57 cm and a source-to-detector distance of 104 cm.

HVL Measurements—To quantify the photon beam hardness and energy spectrum, it was necessary to perform half-value-layer (HVL) measurements of the photons coming out of the face of the collimators. These measurements are essential to determine the inherent and bow-tie filtration properties for the scanner. The gantry was parked so that the X-ray tube remained stationary at the 6 o'clock position. The ion chamber remained stationary and fixed at isocenter along the central axis directly above the X-ray tube. The table was not in the beam path. As for any HVL measurements, an initial exposure without filtration was obtained first. Thin sheets (1.0 mm) of type-1100 high-purity aluminum were added as repeated exposure measurements were taken until the reading was less than half of the initial value. Then all sheets were removed, and another measurement without filtration was taken as a check. Fig. 1 shows our HVL measurement setup.

Equivalent Spectrum Generation—Using Boone and Seibert's tungsten anode spectral model of interpolated polynomials (TASMIPs) (Boone and Seibert 1997), an initial soft tungsten spectrum was obtained for 100 kVp and 120 kVp without added filtration and with zero percent voltage ripple. A detailed explanation of the method to obtain an equivalent spectrum is provided in Turner *et al*. (2009). Briefly, (1) the initial soft tungsten spectrum is transmitted through a very thin and uniform sheet of hardening material. Aluminum was chosen for our purposes. Assuming exponential attenuation, this produces a “candidate spectrum.” (2) The candidate spectrum is transmitted through the central ray of the bow-tie filter, and the air KERMA is calculated. (3) The resulting transmitted spectrum is next

transmitted through a very thin and uniform sheet of aluminum, and the air KERMA is calculated again. (4) The third step is repeated iteratively while increasing the thickness of aluminum by 1 micron until the air KERMA is one-half of the initial air KERMA value in the second step. Photon mass-attenuation coefficients (μ/ρ) and mass energy-absorption coefficients (μ_{en}/ρ) (Hubbell and Seltzer 1996) were used to perform exponential attenuation and KERMA was calculated as

$$\mathrm{KERMA}=\Psi\left(\frac{\mu_{\mathrm{en}}}{\rho}\right), \quad (1)$$

where Ψ (J m^{-2}) is the energy fluence of photons passing through the area of the absorbing material, and (μ_{en}/ρ) is the mass energy-absorption coefficient for mono-energetic photons. The total air KERMA of a spectrum was calculated by summing over all energies as

$$\mathrm{KERMA}_{\mathrm{total}}=\sum_i n_i\Psi_i\left(\frac{\mu_{\mathrm{en}}}{\rho}\right)_i, \quad (2)$$

where n_i is the number of photons in each bin, Ψ_i is the corresponding energy fluence, and $(\mu_{en}/\rho)_i$ is the mass energy-absorption coefficient for each energy, i.

Bow-tie Profile Measurements—The Philips Brilliance 64 has a single bow-tie filter that was modeled by following the procedure in Turner *et al*. (2009). Measurements of the bow-tie filter profile were used to determine the real spectrum's attenuation across the photon beam due to the bow-tie geometry and filtration. The gantry was parked with the tube in the 3 o'clock position in order to eliminate attenuation due to the exam table. The ion chamber was clamped to a ring stand, and exposure measurements were taken every 1 cm starting at isocenter by incrementally moving the table up in order to determine the attenuation in exposure from bow-tie filter center to edge. Measurements were taken for the upper half of the bow-tie filter, and it was assumed symmetric about the central axis (Fig. 2).

Using this attenuation profile, we iteratively determined the bow-tie-filter path length as a function of distance across the bow-tie filter (transverse direction) (Turner *et al.* 2009). All routines were coded in MATLAB R2012b (Mathworks). This was done for each equivalent spectra determined in the previous section.

Experimental Measurements

CT Pencil Ionization Chamber Measurements—A standard 100-mm long CT pencil ionization chamber (Fluke Biomedical Model 8000 chamber with NERO Max, Fluke Biomedical, Everett, WA) was used to take exposure measurements in air, as well as in 16-cm and 32-cm acrylic CTDI dose phantoms at isocenter for center and peripheral (12 o'clock) positions. Measurements were collected for 100 and 120 kVp at 300 mAs. At least three unique measurements were made for each energy, mAs, and collimation combination. The average of these exposure readings was used for purposes of calculating the dose to the chamber. These were converted to standard computed-tomography dose indices ($CTDI_{100}$) following AAPM Report 96. These were calculated as:

$$\mathrm{CTDI}_{100} = \frac{f \times C \times L \times X}{nT}, \quad (3)$$

where f is the exposure-to-dose conversion factor for air (8.7 mGy R^{-1}), C is the chamber calibration factor (0.31 for our chamber), L is the active length of the pencil ionization chamber (100 mm), X is exposure in R, n is the number of detector elements, and T is the size of a detector element.

Simulations in Air, 16-cm, and 32-cm Dose Phantoms—Next we modeled our CTDI measurements in the Monte Carlo simulation. A thin-walled ionization chamber was constructed from manufacturer specifications. For our particular model of ion chamber, the wall is made of PMMA and the active volume is 10.1 cm^3 with a sensitive length of 10.0 cm. The chamber outside diameter measures 12.7 mm ± 0.4 mm, and the chamber inside diameter is 11.44 mm. To model the chamber in our simulations, an inner diameter of 11.5 mm and outer diameter of 12.5 mm were used. Each voxel measured 0.5 × 0.5 × 2.5 mm^3. The PMMA dose phantom itself and the air in the active chamber volume were identified as separate regions. Energy deposited into the air chamber was scored in the simulation and used to calculate simulated dose.

All physical densities and elemental compositions of the materials modeled in our system geometry were taken from NIST database definitions (Coursey *et al.* 2010) (Table 1). Poly(methyl methacrylate) (PMMA, $(C_5O_2H_8)_n$) was used to model the CTDI acrylic dose phantoms in the simulations. The exam table was modeled as pure carbon composition, as the exact chemical composition was considered proprietary information. The composition of air was used for both surrounding outside air in the simulation as well as the air in the modeled ionization chamber.

Monte Carlo Normalization Factor—We compared the real CTDI_{100} measurements in air to the simulated CTDI_{100} values in air to derive normalization factors for 100 and 120 kVp at a nominal beam collimation of 64 × 0.625 mm (40 mm). Our Monte Carlo normalization factor, K, as a function of energy is described by:

$$K_E = \frac{D_{\mathrm{air,measured}_E}}{D_{\mathrm{air,simulated}_E}}. \quad (4)$$

Measurements Reported by OSL Dosimeters—We exposed several linear arrays of optically stimulated luminescence (OSL) dosimeters manufactured by Landauer, Inc. (Landauer 2006). The dosimeter material is housed in a black polycarbonate case, and the length of the OSL strip inside is 150 mm long and 0.4 mm thick. The dosimeter material is a polymer substrate of aluminum oxide doped with carbon (Al_2O_3:C). According to the manufacturer, these OSL dosimeters can measure radiation doses of 0.01 mGy or less, and less than 0.2% of the signal is erased when a dosimeter is read (Landauer 2006).

Results

The measured HVL on the Philips 64-slice Brilliance scanner was 7.6 ± 0.2 mm of Al for 100 kVp and 9.0 ± 0.2 mm Al for 120 kVp. The measured bow-tie filter attenuation profile at system isocenter is shown in Fig. 3, and a sample of the spatial distribution dependence of photons is shown in Fig. 4.

CTDI Measurements

The measured and simulated $CTDI_{100}$ in air at isocenter for a single axial scan taken at 100 and 120 kVp and 300 mAs are presented in Table 2. $CTDI_{100}$ center values were calculated using Equation 3. Normalization factors were derived by taking the ratio of the measured dose to the simulated dose in air for each nominal kVp. In our present study, we consider only one nominal beam collimation of 64 × 0.625 mm (40 mm). The normalization factors were used to convert the dose simulated to absolute absorbed dose for 100 and 120 kVp and our particular beam collimation.

As mentioned in the previous section, the simulated CT X-ray source moves in one-degree increments with 100,000 primary photons per step. Multiple simulations were performed and achieved overall relative errors of 0.5% or less in the specified detector regions in the simulation. To obtain the total error in our normalization factors and CTDI values, error from the simulation was propagated with the manufacturer-specified 5% error in our ion chamber measurements.

The results of the $CTDI_{100}$ measurements and simulations are presented in Table 3 for 100 kVp and Table 4 for 120 kVp. Differences on the order of $< 10 \mu Gy\ mAs^{-1}$ are observed. The uncertainties in the ionization chamber measurements are reported at the level of 5%, according to the manufacturer. Errors on the simulated values are reported as the Monte Carlo associated relative error of each particular detector region in the simulation.

Results for $CTDI_{100}$ measurements from the OSL dosimeters and the ionization chamber are reported in Table 5 for 100 kVp and Table 6 for 120 kVp. We also compared our observed differences to previous differences observed by other authors. For 120 kVp, the percent differences observed are on par with those observed by Vrieze *et al.* (2012) and observed to be approximately less than 10% in the majority of cases. The OSLs appear to show some under response in the air-only and peripheral measurement cases, but tend to overestimate dose when compared to the ion chamber in the center regions. However, for 100 kVp, we tend to see more over response in all cases, but unfortunately did not have other previous results to compare to for 100 kVp. It should be noted that our measurements were not intended as an exhaustive comparison study of OSL versus ionization chamber measurements. The values reported by other authors are intended as a descriptive tool to compare our observed results.

Dose Profiles

The OSL dose profile reported by the manufacturer in air at 120 kVp and 300 mAs allowed direct measurement of the realistic beam width including effects of penumbra. We found that the actual beam width was 42.1 mm, slightly larger than our nominal beam width of 40

mm. By having this knowledge, we were able to model the actual beam width in our simulations. Fig. 5a shows our dose profile in air modeled for our 100 kVp spectra, and Fig. 5b illustrates the comparison between the 120 kVp OSL profile in air and our simulated profile in air, allowing us to confirm that the beam widths indeed match. The discrepancy of the dose magnitude between the OSL and GEANT4 profile is due to the difference in the reported dose in air, with the OSL underreporting dose compared to the ion chamber. The ionization chamber measured values were used as the standard in the derivation of our normalization factors. The discussion section also assesses the observed discrepancies between OSL and ion chamber values.

Figs. 6a-d illustrate our results for the 16-cm head and 32-cm body phantoms for dose profiles at the center position in the phantoms. The dose profiles from the OSL dosimeter measurements taken in those regions, as reported by the manufacturer, are plotted on top of our dose profiles obtained from the model simulation.

Discussion

The GEANT4 simulation environment is very flexible and has been extensively verified. We have used it previously to simulate internal sources of radiation (Stabin *et al*. 2012); its use for external radiation sources, particularly to simulate a CT scanner has been demonstrated by others as well as other medical physics applications (e.g. Archambault *et al.* 2003, Jiang and Paganetti 2004). We show here a simulated CT source modeled after a Philips Brilliance 64, with a bow-tie filter. We were not able to obtain actual spectral data from the manufacturer, so we modeled a reasonable X-ray spectrum based on methods from literature and experimental data. Our simulated X-ray spectrum showed excellent agreement (differences of $< 10 \mu Gy\ mAs^{-1}$) with the independently measured ionization chamber results.

We calibrated our simulations against ion chamber measurements in acrylic phantoms. The ion chamber measurements and simulation results show reasonable agreement with an overall average percent difference of 6% in the CTDI values. For both nominal kVp values, the simulated CTDI values tend to overestimate the measured CTDI values in the 32-cm body phantom. However, for the 16-cm head phantom, the simulated CTDI values tend to under predict the measured values slightly. Some differences between the simulation and real-world measurements could be due to accuracy in the X-ray spectra, filtration, and geometry modeled. Also, beam hardening in the simulated spectra may be responsible for these observed results. Uncertainties in the geometry and modeling of the table material could be contributing factors, as there is non-negligible attenuation through the table. There may be differences between our simulated and measured results due to the ideal assumption of using point-source geometry in our Monte Carlo simulation. We did not take focal-spot size into account when modeling our CT source. Despite these sources of error, we find acceptable agreement between our measured and simulated results in order to validate our model.

Random errors in the simulated dose may have contributed to the differences observed as well as uncertainty in the normalization factors used to calculate dose. The normalization

factors derived from in-air measurements are used to convert all of our simulated results. There is a 5% uncertainty in all of the ionization chamber measurements, and when coupled with the uncertainty in the simulation (Monte Carlo associated relative error of 0.5% or less), there is a greater than 5% error in our absolute dose results reported. Although we performed 50-150 runs per geometry with 100,000 primary photons per one-degree increment, some of our plots indicate our data still contain noise. The amount of noise present is due to scoring in air, which is very low density. Nonetheless, the results agree well with the measured values, and a smoothed profile can express the true nature of the results (e.g. Figs. 5 and 6).

Other researchers have observed similar discrepancies between these particular manufactured OSL dosimeters and ionization chamber measurements. Lavoie *et al.* (2011) found that OSL dosimeter energy response decreased with increased tube voltage. For 135 kVp, they report a -15.5% difference when compared to a NIST-traceable calibrated ionization chamber, whereas for 80 kVp the percent difference was only -2.0%. Vrieze *et al.* (2012) revealed for 120 kVp measurements taken at the center position, that deviations of 10.4% were observed in the 32-cm acrylic phantom and 3.6% in the 16-cm phantom. Similar to our in-air results, they found a deviation of -9.9% at 120 kVp (where we saw a difference of -7.8%). Therefore, we suggest that the percent differences observed for our experiments are comparable to results observed by other authors.

The aluminum oxide-based OSL material has an energy-dependent response, and a correction factor is necessary to achieve high accuracy in the dose results. Variables such as tube voltage, phantom size and material, and position within the phantom could influence the interaction of the beam with the dosimeters (Vrieze *et al*. 2012). While it is assumed that the manufacturer-reported results from the OSL dosimeters take into account a suitable energy-dependent correction factor, this is not known with absolute certainty. Hence, this could account for some discrepancies observed between the OSL and ion chamber results in the present work and those of other authors.

These results demonstrate that Monte Carlo models for multi-detector CT can be used to accurately determine patient dose at a voxel level. We will apply our calibrated Monte Carlo simulation to determine organ doses and effective dose values for patients previously given CT examinations at Vanderbilt Medical Center. The application of our calibrated GEANT4 radiation transport code for CT dosimetry to pediatric patient data as well as a series of deformable phantoms will be the subject of future publications.

Conclusion

We have developed and tested a new Monte Carlo code using the GEANT4 toolkit to simulate patients undergoing a CT examination. In order to accurately model the complexity of the X-ray beam and CT geometry, measurements of the beam half-value layer, bow-tie filter attenuation and physical characteristics of the CT scanner model are required. We calibrated our method to physical dose measurements made in air with a pencil ionization chamber by deriving photon fluence normalization factors for 100 and 120 kVp. Absorbed

dose values and profiles determined from simulation were in overall agreement to within 6% of measured values.

We have begun to apply our GEANT4 simulation to calculate both organ and effective doses for pediatric patients undergoing CT examinations. Future work is focused on using anthropomorphic phantoms in the Monte Carlo simulation to determine individual organ and effective doses for a pediatric population for a range of percentiles and underweight and obese individuals. This will provide a method for predicting CT dose prior to irradiation of a patient and help to develop scanning protocols that minimize dose without compromising image quality.

Acknowledgments

Research supported under NIH/NCI 1 R01 CA155400-01A1.

References

Agostinelli S, Allison J, Amako K, Apostolakis J, Araujo H, Arce P, Asai M, Axen D, Banerjee S, Barrand G, Behner F, Bellagamba L, Boudreau J, Broglia L, Brunengo A, Burkhardt H, Chauvie S, Chuma J, Chytracek R, Cooperman G, Cosmo G, Degtyarenko P, Dell'Acqua A, Depaola G, Dietrich D, Enami R, Feliciello A, Ferguson C, Fesefeldt H, Folger G, Foppiano F, Forti A, Garelli S, Giani S, Giannitrapani R, Gibin D, Gómez Cadenas JJ, González I, Gracia Abril G, Greeniaus G, Greiner W, Grichine V, Grossheim A, Guatelli S, Gumplinger P, Hamatsu R, Hashimoto K, Hasui H, Heikkinen A, Howard A, Ivanchenko V, Johnson A, Jones FW, Kallenbach J, Kanaya N, Kawabata M, Kawabata Y, Kawaguti M, Kelner S, Kent P, Kimura A, Kodama T, Kokoulin R, Kossov M, Kurashige H, Lamanna E, Lampén T, Lara V, Lefebure V, Lei F, Liendl M, Lockman W, Longo F, Magni S, Maire M, Medernach E, Minamimoto K, Mora de Freitas P, Morita Y, Murakami K, Nagamatu M, Nartallo R, Nieminen P, Nishimura T, Ohtsubo K, Okamura M, O'Neale S, Oohata Y, Paech K, Perl J, Pfeiffer A, Pia MG, Ranjard F, Rybin A, Sadilov S, Di Salvo E, Santin G, Sasaki T, Savvas N, Sawada Y, Scherer S, Sei S, Sirotenko V, Smith D, Starkov N, Stoecker H, Sulkimo J, Takahata M, Tanaka S, Tcherniaev E, Safai Tehrani E, Tropeano M, Truscott P, Uno H, Urban L, Urban P, Verderi M, Walkden A, Wander W, Weber H, Wellisch JP, Wenaus T, Williams DC, Wright D, Yamada T, Yoshida H, Zschiesche D. Geant4 Collaboration. GEANT4—a simulation toolkit. Nuclear Instruments and Methods in Physics Research Section A: Accelerators, Spectrometers, Detectors and Associated Equipment. 2003; 506(3):250–303.10.1016/S0168-9002(03)01368-8

Allison J, Amako K, Apostolakis J, Araujo H, Dubois PA, Asai M, Barrand G, Capra R, Chauvie S, Chytracek R, Cirrone GAP, Cooperman G, Cosmo G, Cuttone G, Daquino GG, Donszelmann M, Dressel M, Folger G, Foppiano F, Generowicz J, Grichine V, Guatelli S, Gumplinger P, Heikkinen A, Hrivnacova I, Howard A, Incerti S, Ivanchenko V, Johnson T, Jones F, Koi T, Kokoulin R, Kossov M, Kurashige H, Lara V, Larsson S, Lei F, Link O, Longo F, Maire M, Mantero A, Mascialino B, McLaren I, Lorenzo PM, Minamimoto K, Murakami K, Nieminen P, Pandola L, Parlati S, Peralta L, Perl J, Pfeiffer A, Pia MG, Ribon A, Rodrigues P, Russo G, Sadilov S, Santin G, Sasaki T, Smith D, Starkov N, Tanaka S, Tcherniaev E, Tome B, Trindade A, Truscott P, Urban L, Verderi M, Walkden A, Wellisch JP, Williams DC, Wright D, Yoshida H. Geant4 developments and applications. IEEE Transactions on Nuclear Science. 2006; 53(1):270–278.10.1109/TNS.2006.869826

Archambault L, Beaulieu L, Carrier JF, Castrovillari F, Chauvie S, Foppiano F, Ghiso G, Guatelli S, Incerti S, Lamanna E, Larsson S, Lopes MC, Peralta L, Pia MG, Rodrigues P, Tremblay VH, Trindade A. Overview of Geant4 applications in medical physics. Nuclear Science Symposium Conference Record, 2003 IEEE. 2003; 3:1743–1745.10.1109/NSSMIC.2003.1352215

Boone JM, Seibert JA. An accurate method for computer-generating tungsten anode x-ray spectra from 30 to 140 kV. Medical Physics. 1997; 24:1661–1670.10.1118/1.597953 [PubMed: 9394272]

Brenner DJ, Elliston CD, Hall EJ, Berdon WE. Estimated risks of radiation-induced fatal cancer from pediatric CT. American journal of roentgenology. 2001; 176(2):289–296.10.2214/ajr.176.2.1760289 [PubMed: 11159059]

Coursey, J.; Schwab, D.; Tsai, J.; Dragoset, R. National Institute of Standards and Technology; Gaithersburg, MD: 2010. Atomic weights and isotopic compositions (version 3.0). [online] available: http://physics.nist.gov/comp [2013 july 15]

DeMarco J, Cagnon C, Cody D, Stevens D, McCollough C, O'Daniel J, McNitt-Gray M. A Monte Carlo based method to estimate radiation dose from multidetector CT (MDCT): cylindrical and anthropomorphic phantoms. Phys Med Biol. 2005; 50(17):3989.10.1088/0031-9155/50/17/005 [PubMed: 16177525]

DeMarco J, Cagnon C, Cody D, Stevens D, McCollough C, Zankl M, Angel E, McNitt-Gray M. Estimating radiation doses from multidetector CT using Monte Carlo simulations: effects of different size voxelized patient models on magnitudes of organ and effective dose. Phys Med Biol. 2007; 52(9):2583.10.1088/0031-9155/52/9/017 [PubMed: 17440254]

Diagnostic Imaging Council CT Committee Task Group #23. The measurement, reporting, and management of radiation dose in CT. AAPM Report. 2008; 96

Dixon RL. A new look at CT dose measurement: beyond CTDI. Med Phys. 2003; 30:1272.10.1118/1.1576952 [PubMed: 12852553]

Donnelly LF. Reducing radiation dose associated with pediatric CT by decreasing unnecessary examinations. American Journal of Roentgenology. 2005; 184(2):655–657.10.2214/ajr.184.2.01840655 [PubMed: 15671393]

Donnelly LF, Emery KH, Brody AS, Laor T, Gylys-Morin VM, Anton CG, Thomas SR, Frush DP. Minimizing radiation dose for pediatric body applications of single-detector helical CT strategies at a large children's hospital. American Journal of Roentgenology. 2001; 176(2):303–306.10.2214/ajr.176.2.1760303 [PubMed: 11159061]

Goske MJ, Applegate KE, Boylan J, Butler PF, Callahan MJ, Coley BD, Farley S, Frush DP, Hernanz-Schulman M, Jaramillo D, Johnson ND, Kaste SC, Morrison G, Strauss KJ, Tuggle N. The 'Image Gently' campaign: increasing CT radiation dose awareness through a national education and awareness program. Pediatric Radiology. 2008; 38(3):265–269.10.1007/s00247-007-0743-3 [PubMed: 18202842]

International Commission on Radiological Protection. 1990 Recommendations of the International Commission on Radiological Protection. Ann ICRP. 1991; 21(1-3) ICRP Publication 60.

International Commission on Radiological Protection. Managing Patient Dose in Multi-Detector Computed Tomography (MDCT). Ann ICRP. 2007; 37(1) ICRP Publication 102.

International Commission on Radiological Protection. The 2007 Recommendations of the International Commission on Radiological Protection. Ann ICRP. 2007; 37(2-4) ICRP Publication 103.

Jarry G, DeMarco J, Beifuss U, Cagnon C, McNitt-Gray M. A Monte Carlo-based method to estimate radiation dose from spiral CT: from phantom testing to patient-specific models. Phys Med Biol. 2003; 48:2645.10.1088/0031-9155/48/16/306 [PubMed: 12974580]

Jiang H, Paganetti H. Adaptation of GEANT4 to Monte Carlo dose calculations based on CT data. Medical physics. 2004; 31(10):2811–2818.10.1118/1.1796952 [PubMed: 15543788]

Hubbell, JH.; Seltzer, SM. Tables of X-ray mass attenuation coefficients and mass energy-absorption coefficients. National Institute of Standards and Technology; 1996.

Landauer, Inc. Optically stimulated luminescence dosimetry for computed tomography—measurement of CTDI and dose profiles. Landauer, Inc.; 2 Science Road, Glenwood, Illinois 60425: 2006.

Lavoie L, Ghita M, Brateman L, Arreola M. Characterization of a commercially available, optically-stimulated luminescent dosimetry system for use in computed tomography. Health Physics. 2011; 101(3):299–310.10.1097/HP.0b013e31820f8e0e [PubMed: 21799346]

Lee C, Lee C, Staton RJ, Hintenlang DE, Arreola MM, Williams JL, Bolch WE. Organ and effective doses in pediatric patients undergoing helical multislice computed tomography examination. Medical Physics. 2007; 34(1858)10.1118/1.2723885

Lee C, Lodwick D, Williams JL, Bolch WE. Hybrid computational phantoms of the 15-year male and female adolescent: applications to CT organ dosimetry for patients of variable morphometry. Medical Physics. 2008; 35:2366.10.1118/1.2912178 [PubMed: 18649470]

Li X, Samei E, Segars WP, Sturgeon GM, Colsher JG, Frush DP. Patient-specific radiation dose and cancer risk for pediatric chest CT. Radiology. 2011; 259(3):862–874.10.1148/radiol.11101900 [PubMed: 21467251]

Li X, Samei E, Segars WP, Sturgeon GM, Colsher JG, Toncheva G, Yoshizumi TT, Frush DP. Patient-specific radiation dose and cancer risk estimation in CT: Part I. Development and validation of a Monte Carlo program. Medical Physics. 2011; 38(1):397.10.1118/1.3515839 [PubMed: 21361208]

Li X, Samei E, Segars WP, Sturgeon GM, Colsher JG, Toncheva G, Yoshizumi TT, Frush DP. Patient-specific radiation dose and cancer risk estimation in CT: Part II. Application to patients. Medical Physics. 2011; 38(1):408.10.1118/1.3515864 [PubMed: 21361209]

Linton OW, Mettler F Jr. A National conference on dose reduction in CT, with an emphasis on pediatric patients. American Journal of Roentgenology. 2003; 181(2):321–329. [PubMed: 12876005]

MathWorks, Inc.. MATLAB and Statistics Toolbox Release R. Natick, Massachusetts, United States: 2012b.

Schauer, DA.; Linton, OW. NCRP report no 160, ionizing radiation exposure of the population of the United States, medical exposure-are we doing less with more, and is there a role for health physicists?. NCRP; Bethesda, MD: 2009.

Stabin M, Emmons MA, Segars WP, Fernald MJ. Realistic reference adult and paediatric phantom series for internal and external dosimetry. Radiation Protection Dosimetry. 2012; 149(1):49–55.10.1093/rpd/ncr383 [PubMed: 22262819]

Strauss KJ, Goske MJ, Frush DP, Butler PF, Morrison G. Image gently vendor summit: working together for better estimates of pediatric radiation dose from CT. American Journal of Roentgenology. 2009; 192(5):1169–1175.10.2214/AJR.08.2172 [PubMed: 19380538]

Turner AC, Zhang D, Kim HJ, DeMarco JJ, Cagnon CH, Angel E, Cody DD, Stevens DM, Primak AN, McCollough CH, McNitt-Gray MF. A method to generate equivalent energy spectra and filtration models based on measurement for multidetector CT Monte Carlo dosimetry simulations. Medical physics. 2009; 36.6:2154–2164.10.1118/1.3117683 [PubMed: 19610304]

Vrieze TJ, Sturchio GM, McCollough CH. Technical note: Precision and accuracy of a commercially available CT optically stimulated luminescent dosimetry system for the measurement of CT dose index. Medical Physics. 2012; 39(11):6580–6584.10.1118/1.4754591 [PubMed: 23127052]

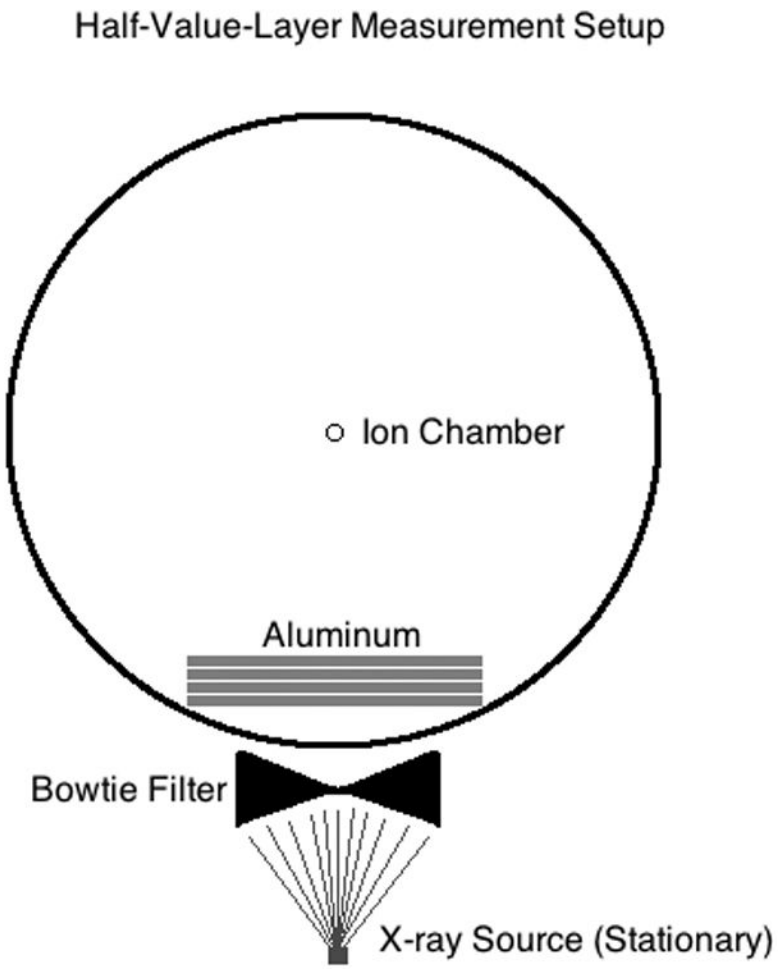

Fig. 1.

Setup for the half-value-layer (HVL) measurements. The scanner gantry was parked with the X-ray tube at the 6 o'clock position. Thin sheets of aluminum were stacked vertically as exposure readings were made.

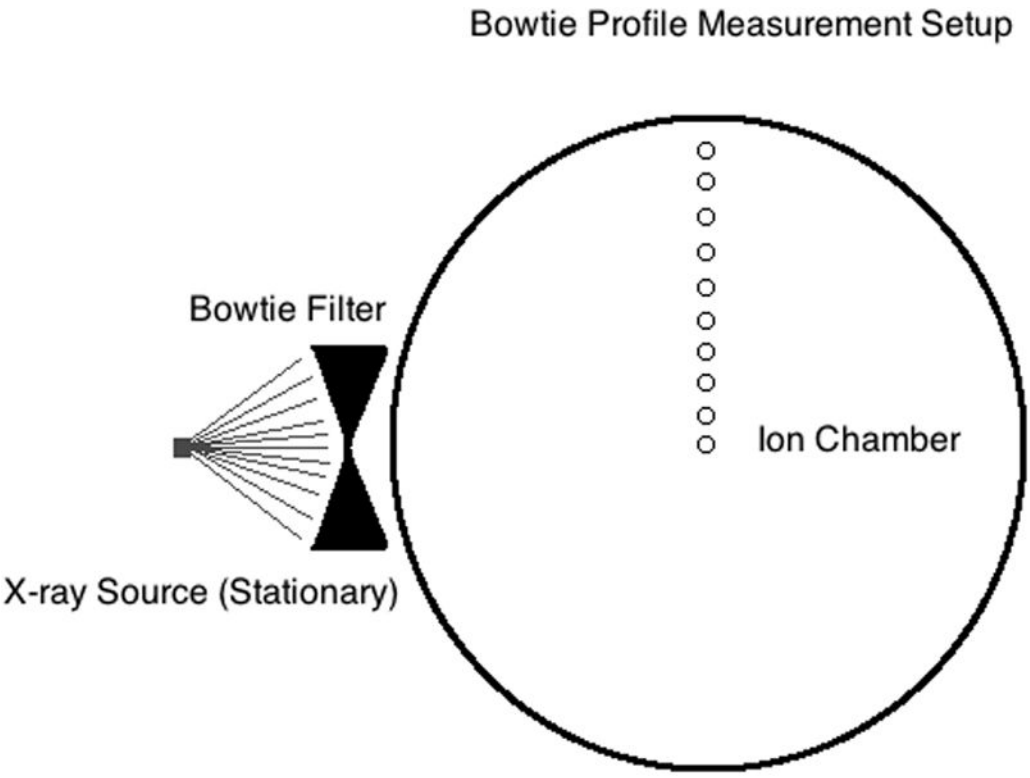

Fig. 2.

Experimental setup for measurements of the bow-tie filter attenuation profile. The CT scanner gantry was parked with the X-ray tube at the 3 o'clock position. Exposure readings were made every 1 cm across the filter starting at isocenter moving towards the edge of the filter.

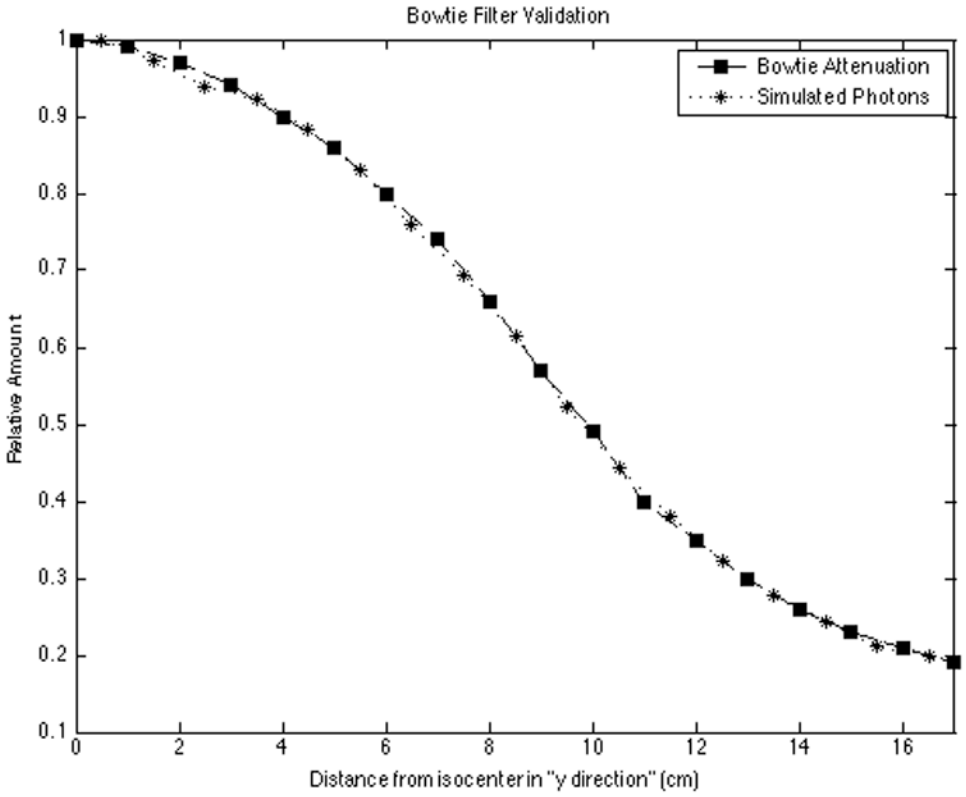

Fig. 3.

The measured bow-tie filter attenuation profile as a result of ionization chamber measurements made every 1 cm moving away from the central ray is plotted with photons generated by the simulation. Simulated photon positions are binned according to their path lengths as a function of their distances relative to the central ray at isocenter. Attenuation measurements are plotted according to bin edges whereas simulated photons are plotted at bin center.

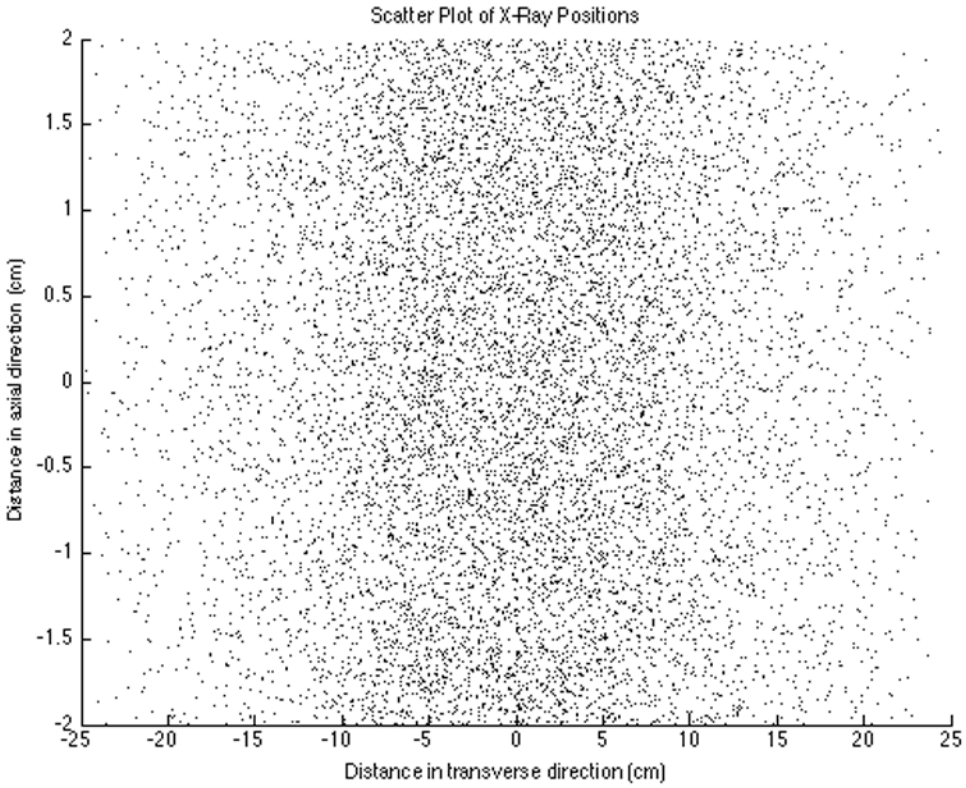

Fig. 4.

The spatial distribution dependence of photons at system isocenter is shown. The distance in the “y-direction” represents the bow-tie filter dependence in the spatial distribution. The “z-direction” is across the other direction of the face of the collimators. The “x-direction” would be into the page and in the direction towards the simulated phantom or patient.

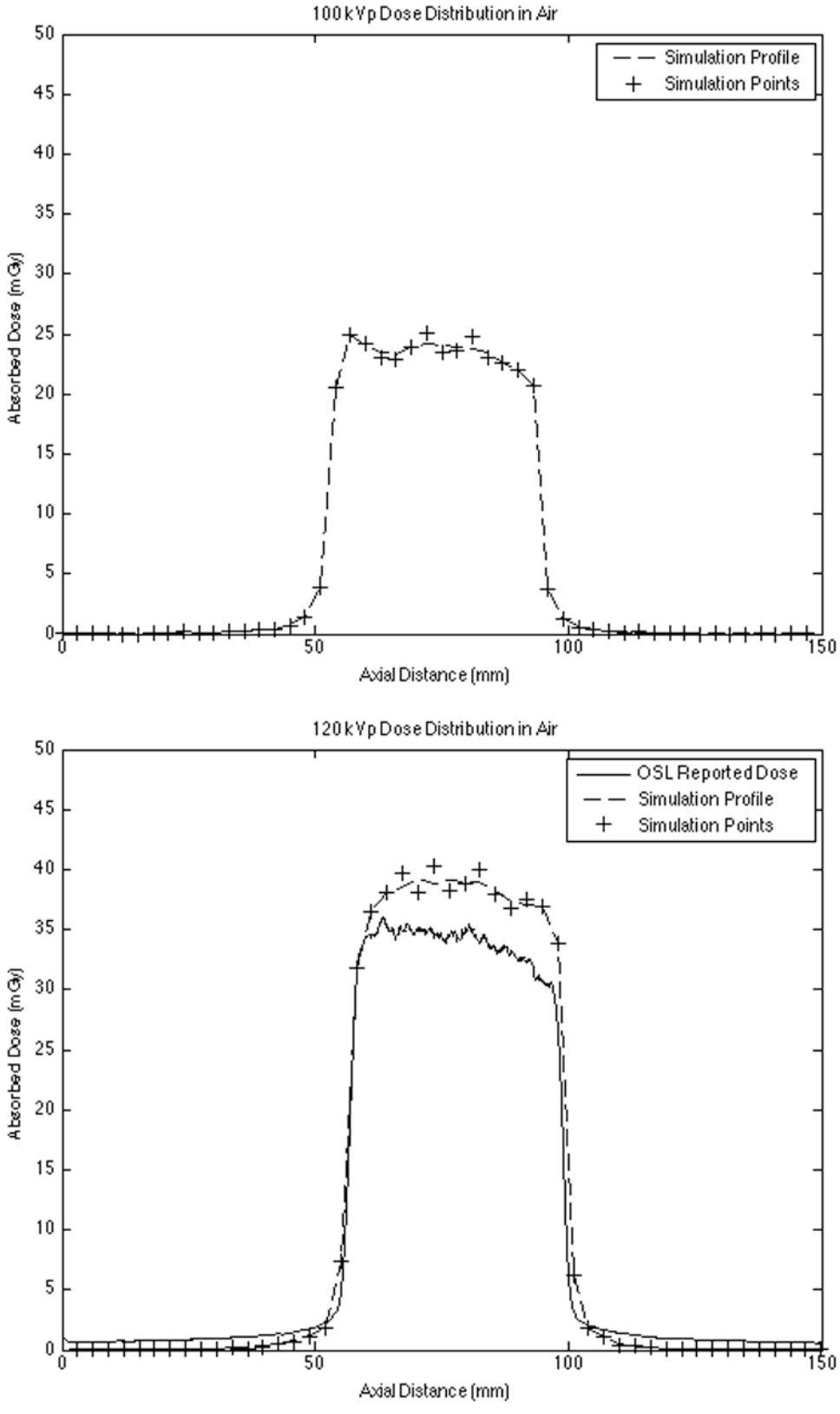

Fig. 5.

Simulated dose distributions in air for (a) 100 kVp and (b) 120 kVp, at 300 mAs. The distribution for 120 kVp also shows the dose profile obtained from an OSL dosimeter exposed in air at 120 kVp. The comparison between the two methods provides confirmation of the match between the observed beam width (42.1 mm) and the beam width generated from simulation.

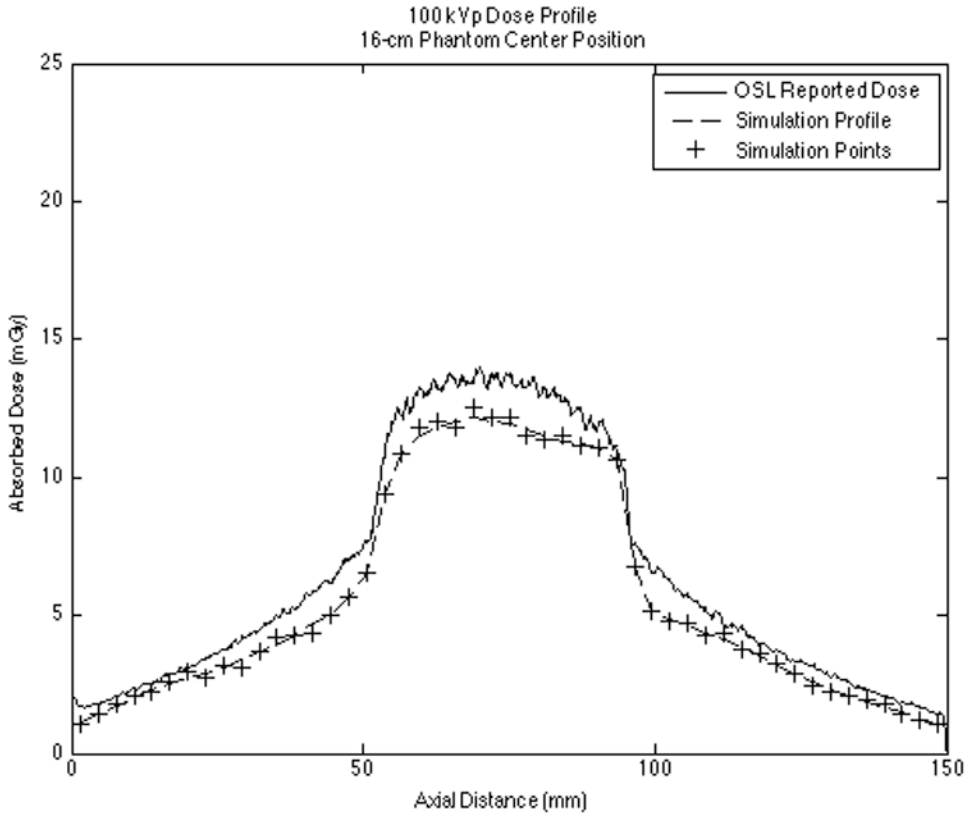

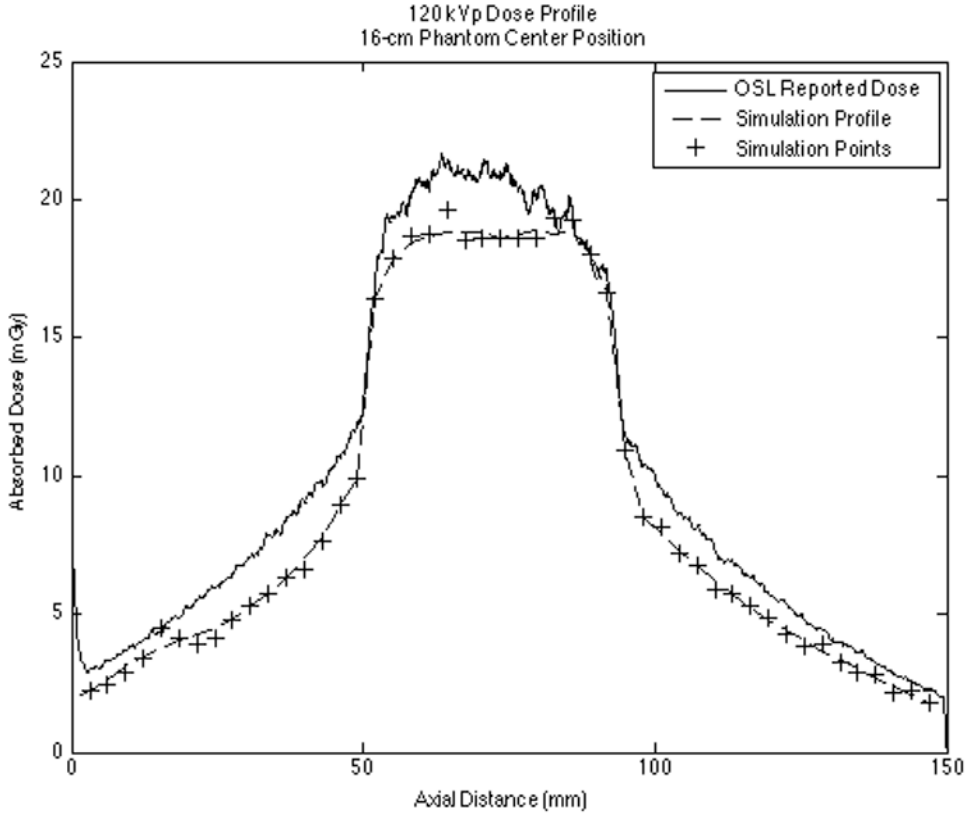

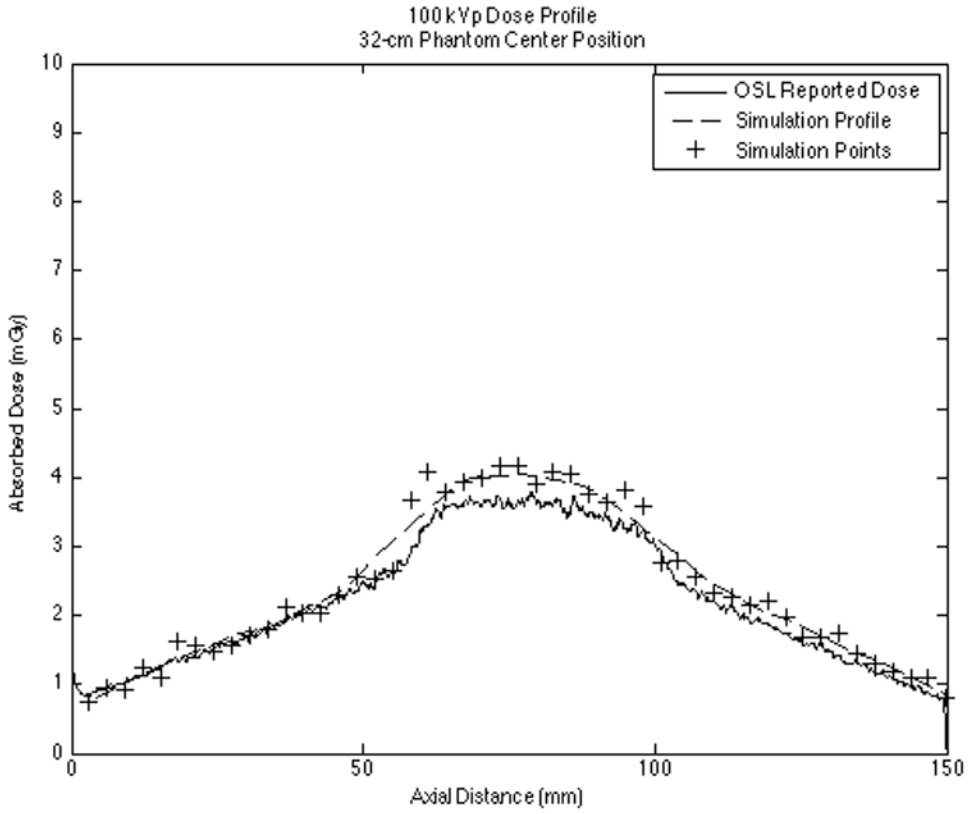

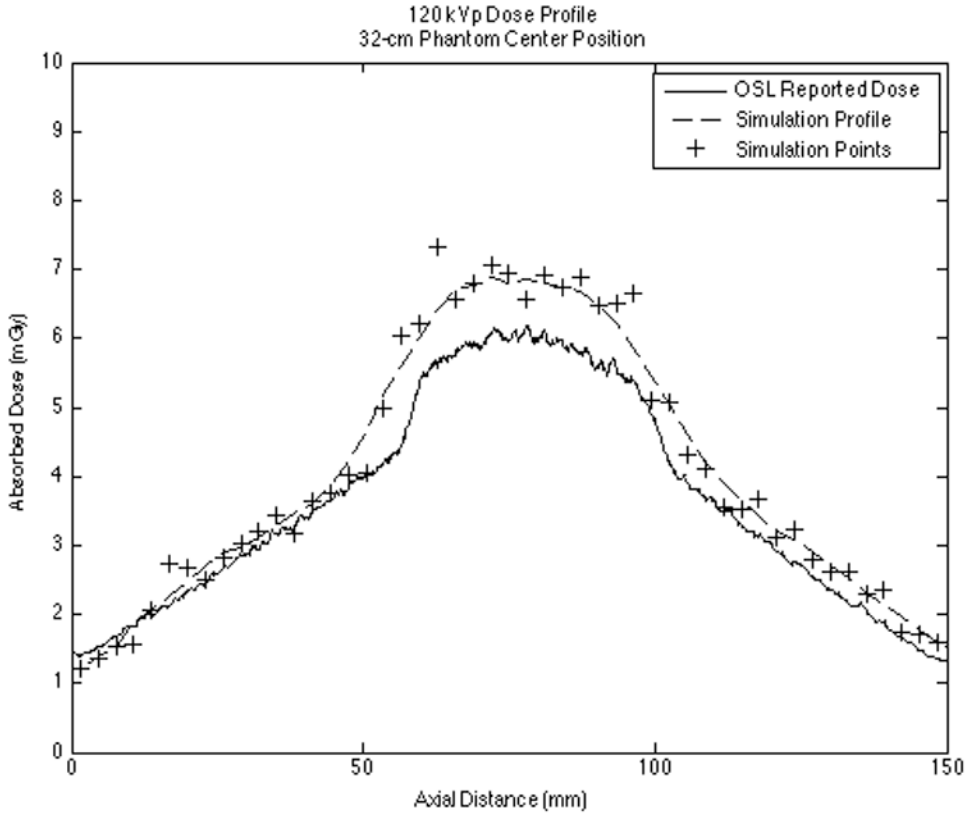

Fig. 6.

(a) The dose profile for the 16-cm CTDI phantom results for 100 kVp at the center position and (b) shows the dose profile for the 16-cm CTDI phantom results at 120 kVp. (c) The dose profile for the 32-cm CTDI phantoms at the center position for 100 kVp, and (d) shows the dose profile in the 32-cm phantom center case for 120 kVp. In all cases, the dose profile obtained from the OSL dosimeter reported by Landauer is shown as a solid black line, the simulation data points from GEANT4 are shown as plus signs, and the smoothed GEANT4 profile is shown as a dashed black line.

Table 1

Summary of materials used in the Monte Carlo simulation model. Material compositions are taken from the NIST database (Coursey *et al.* 2010).

Material	Density (g cm^{-3})	Chemical Composition (% by mass)				
		H	C	N	O	Elements Z > 8
Air	1.20×10^{-3}		0.012	75.53	23.18	Ar (1.28)
Exam Table	2.27		100			
PMMA	1.19	8.05	59.99		31.96	

Table 2

Measured and simulated $CTDI_{100}$ in air at isocenter and derived normalization factors are reported for 100 and 120 kVp for a nominal beam collimation of 40 mm.

Energy (kVp)	Measured $CTDI_{100}$ in air (10^{-2} mGy mAs^{-1})	Simulated $CTDI_{100}$ in air (10^{-12} mGy $particle^{-1}$)	Normalization factor (10^{10} particle mAs^{-1})
100	8.47 ± 0.42	2.17 ± 0.0067	3.91 ± 0.20
120	13.7 ± 0.68	2.32 ± 0.0074	5.91 ± 0.30

Table 3

Comparison of $CTDI_{100}$ measurements from the ion chamber to simulated CTDI values in GEANT4 at a nominal tube voltage of 100 kVp for a nominal beam collimation of 40 mm.

	Center Position		
Phantom	**Ion chamber $CTDI_{100}$ (10^{-2} mGy mAs^{-1})**	**Simulated $CTDI_{100}$ (10^{-2} mGy mAs^{-1})**	**Difference (10^{-2} mGy mAs^{-1})**
16-cm CTDI head	6.3 ± 0.32	6.2 ± 0.31	-0.1
32-cm CTDI body	2.0 ± 0.10	2.4 ± 0.12	0.4

Table 4

Comparison of $CTDI_{100}$ measurements from the ion chamber to simulated CTDI values in GEANT4 at a nominal tube voltage of 120 kVp for a nominal beam collimation of 40 mm.

	Center Position		
Phantom	**Ion chamber $CTDI_{100}$ (10^{-2} mGy mAs^{-1})**	**Simulated $CTDI_{100}$ (10^{-2} mGy mAs^{-1})**	**Difference (10^{-2} mGy mAs^{-1})**
16-cm CTDI head	10.4 ± 0.52	9.7 ± 0.49	-0.7
32-cm CTDI body	3.6 ± 0.18	4.1 ± 0.21	0.5

Table 5

Results of CT OSL and ion chamber $CTDI_{100}$ measurements for a tube potential of 100 kVp at 300 mAs. Percent differences are reported as $(CTDI_{OSL} - CTDI_{ion\ chamber})/ CTDI_{ion\ chamber} \times 100$.

Center Position			
Phantom	**Ion chamber $CTDI_{100}$ (mGy)**	**OSL $CTDI_{100}$ (mGy)**	**Percent diff in mean $CTDI_{100}$ values (%)**
16-cm CTDI head	18.9	21.3	12.7
32-cm CTDI body	6.1	6.7	9.8
12 o'clock Position			
16-cm CTDI head	22.0	24.8	12.7
32-cm CTDI body	11.5	11.0	-4.3

Table 6

Results of CT OSL and ion chamber $CTDI_{100}$ measurements for a tube potential of 120 kVp at 300 mAs. Percent differences are reported as $(CTDI_{OSL} - CTDI_{ion\ chamber})/ CTDI_{ion\ chamber} \times 100$. Vrieze *et al.* (2012) percent differences are reported for a beam width of 28.8 mm.

Center Position				
Phantom	**Ion chamber $CTDI_{100}$ (mGy)**	**OSL $CTDI_{100}$ (mGy)**	**Percent diff in mean $CTDI_{100}$ values (%)**	**Vrieze *et al.* (2012) percent difference (%)**
None (in air)	41.0	37.8	-7.8	-9.9
16-cm CTDI head	31.2	33.0	5.8	3.6
32-cm CTDI body	10.7	11.1	3.7	10.4
12 o'clock Position				
16-cm CTDI head	34.5	35.2	2.0	-5.5
32-cm CTDI body	18.7	17.3	-7.5	-5.0